Journal of
Radiation Protection and Research 2016;41(3):237-244
http://dx.doi.org/10.14407/jrpr.2016.41.3.237

pISSN 2508-1888 | eISSN 2466-2461

Development of a Fission Product Transport Module Predicting the Behavior of Radiological Materials during Severe Accidents in a Nuclear Power Plant

Hyung Seok Kang*, Bo Wook Rhee, Dong Ha Kim

Korea Atomic Energy Research Institute, Daejeon, Korea

ABSTRACT

Background: Korea Atomic Energy Research Institute is developing a fission product transport module for predicting the behavior of radioactive materials in the primary cooling system of a nuclear power plant as a separate module, which will be connected to a severe accident analysis code, Core Meltdown Progression Accident Simulation Software (COMPASS).

Materials and Methods: This fission product transport (COMPASS-FP) module consists of a fission product release model, an aerosol generation model, and an aerosol transport model. In the fission product release model there are three submodels based on empirical correlations, and they are used to simulate the fission product gases release from the reactor core. In the aerosol generation model, the mass conservation law and Raoult's law are applied to the mixture of vapors and droplets of the fission products in a specified control volume to find the generation of the aerosol droplet. In the aerosol transport model, empirical correlations available from the open literature are used to simulate the aerosol removal processes owing to the gravitational settling, inertia impaction, diffusiophoresis, and thermophoresis.

Results and Discussion: The COMPASS-FP module was validated against Aerosol Behavior Code Validation and Evaluation (ABCOVE-5) test performed by Hanford Engineering Development Laboratory for comparing the prediction and test data. The comparison results assuming a non-spherical aerosol shape for the suspended aerosol mass concentration showed a good agreement with an error range of about ±6%.

Conclusion: It was found that the COMPASS-FP module produced the reasonable results of the fission product gases release, the aerosol generation, and the gravitational settling in the aerosol removal processes for ABCOVE-5. However, more validation for other aerosol removal models needs to be performed.

Keywords: Risk management system, Fission product vapors, Aerosol, Severe accident

Original Research

Received July 17, 2015
Revision September 9, 2016
Accepted September 13, 2016

Corresponding author:
Hyung Seok Kang

Korea Atomic Energy Research Institute,
989 Daedeok-daero, Yuseong-gu,
Daejeon 34057, Korea
Tel: +82-42-868-8948,
Fax: +82-42-866-6155
E-mail: hskang3@kaeri.re.kr

JRPR

Introduction

Many radiological materials were released from the Fukushima Daiichi nuclear power plants when severe accidents occurred [1]. The public in Fukushima received damage from the released radiation source [1]. To protect the public from the radiological dose due to the radioactive materials that can be released from a nuclear power plant during a severe accident, a risk management system equipped to evaluate the released radiological materials should be established. Korea Atomic Energy Research Institute (KAERI) is developing a Fission Product (FP) module for predicting the radiological material behavior in the Reactor Coolant System (RCS) of a nuclear power plant as a separate module, which will be connected to a severe accident analysis code, Core Meltdown Progression Accident Simulation Software (COMPASS). COMPASS has been developed by KAERI for simulating the severe accident phenomena of the PWR (Pressurized Water Reactor) [2]. In addition, this FP module will be connected to Severe Accident Containment Analysis Package developed by Future and Challenge Technology [3].

Materials and Methods

The purpose of the COMPASS-FP module is to calculate the transport of the total radioactive aerosol mass by integrating the mass over the whole range of the size distribution of the aerosol particles in the RCS during a severe accident. A governing equation for the rate of mass change of the group-i aerosol (dm_{Ai}/dt) in a control volume consists of four terms representing the aerosol inflow ($W_{Ai,in}$) and outflow ($W_{Ai,out}$), the aerosol deposition ($\lambda_t m_{Ai}$), and the aerosol generation (G_i) as defined Equation 1. To calculate each term in the right-hand side of Eq. 1, the fission product release model with three empirical correlations, the aerosol generation model, and the aerosol transport model were implemented in the COMPASS-FP module. The control volume system simulating the RCS of a nuclear power plant will be discussed later.

$$\frac{dm_{Ai}}{dt} = W_{Ai,\,in} - W_{Ai,\,out} - \lambda_t m_{Ai} + G_i \qquad (1)$$

1. Fission product release model

The FP release model simulates the FP gas release from the reactor core when the core is melted during a severe accident. The mass of the group-i fission product (m_{fi}) in the reactor core decreases according to Equation 2 as the core heat up and melting proceed. The FP release models, CORSOR, CORSOR-M, and CORSOR-O with empirical correlations (Table 1), are used to calculate the fractional release coefficient, K_i (T), in Eq. 2 [4, 5]. The original CORSOR model correlates the fractional release rate in an exponential form. Ai and Bi are empirical coefficients based on experimental data, and T is the core cell component temperature in degrees Celsius [4]. The CORSOR-M model correlates the test data using an Arrhenius form. The values of K_{oi} and Qi for each species are listed for different fission product elements [5, 6]. CORSOR-O uses a single temperature activation energy (55,000 cal·mole^{-1}) that is used for every species [6]. The values for K_o are different and sometimes depend on the extent of cladding oxidation or the gas atmosphere [6].

$$\frac{dm_{fi}}{dt} = -K_i(T)m_{fi} \qquad (2)$$

Figure 1 shows that an example of the calculated release rate coefficient K according to the temperature variations from 1200 K to 3100 K for CsI by CORSOR, CORSOR-M, and CORSOR-O. The prediction results by the three models show a slight difference. This may be explained by the fact that the method and test data used for developing the empirical correlations are slightly different [5].

2. Aerosol generation model

All FP gases released from the reactor core were divided into 8 groups (Table 2) according to chemical properties [7] and used as an input for calculating the aerosol generation in the COMPASS-FP module. We used the CORSOR model for the calculation of the FP gas release because the CORSOR

Table 1. Models for the Release Coefficient [3]

Model	Empirical correlation
CORSOR	$K_i = A^i \exp(B_i T)$ A_i, B_i: empirical coefficient
CORSOR-M	$K_i = K_{oi} \exp(-Q_i/RT)$ Q: activation energy R: universal gas constant
CORSOR-O	$K_i = C_{ki} K_o \exp(-Q_i/RT)$ $C_{ki} = (1-f_{H2})\cdot F_{1i} + f_{H2}\cdot F_{2i}$ F_{1i}: release rate for oxidized fuel condition F_{2i}: release rate for reduced fuel condition f_{H2}: mole fraction of H_2 in the FP gas flow

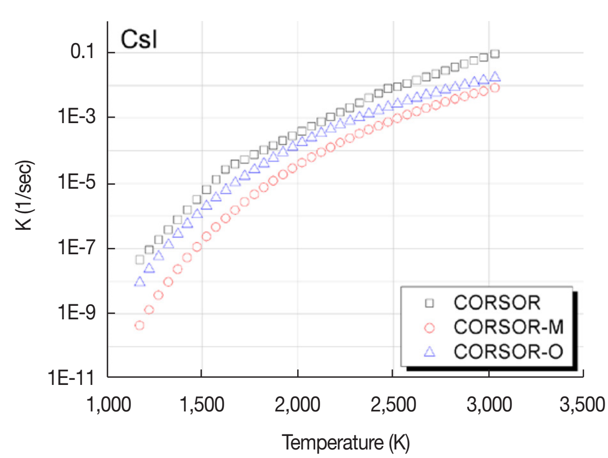

Fig. 1. Compared release rate for CsI by CORSOR, CORSOR-M, and CORSOR-O.

http://dx.doi.org/10.14407/jrpr.2016.41.3.237

Table 2. Melting and Boiling Temperature of Fission Product Vapors [7, 9]

Group	Representatives Species (Member Elements)	Melting Temp. [K]	Boiling Temp. [K]
1	Xe (Kr)	None	None
2	CsI (RbI)	894	1,553
3	CsOH (RbOH)	522	1,263
4	Te (Se, Sb)	723	1,282
5	Sr (Ba)	1,043	1,648
6	Ru (Rh, Pd, Mo, Tc)	2,700	4,392
7	La (Eu, Pr, Nd, Pm, Sm, Gd, Y, Nb, Zr, Ce, Np, Pu)	1,193	3,693
8	Fe (Zr, Cr, Ni, Mn)	1,809	3,148

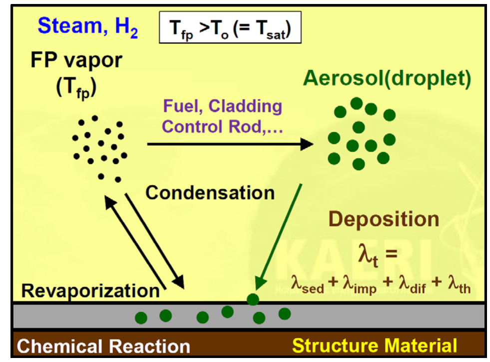

Fig. 2. Concept diagram of aerosol generation and removal.

is a basic model on the basis of the test data. This grouping method can save computation time for calculating the aerosol transport in the RCS. The number of aerosol group will be extended to include important radionuclides including I and Br on the basis of the recent study results including the Fukushima Daiichi accident [1]. Homogeneous nucleation is assumed as the only mechanism of aerosol generation [8]. This model assumes that some fraction of the FP vapors except the noble gas are transformed into liquid droplets depending on their thermodynamic properties (Table 2) and the temperatures of the RCS control volumes to which the FP vapors are discharged. In a real plant, the liquid droplets in an aerosol form are generated with disrupted solid particles of the fuel, cladding, control rod, and structure materials during a severe accident (Figure 2). These solid particles may give an effect on the aerosol shape because the FP vapors can be easily condensed on the surface of the solid particles. However, only the aerosol generation due to the phase change from the vapors to the spherical droplets owing to a thermodynamic condition change of the RCS control volumes was considered in the COMPASS-FP module. The aerosol generation is calculated from combining the mass balance equation of the FP vapors and aerosol droplets with Raoult's law [10] using a numerical iterative method (Equations 3 to 7). The subscript o in the right-hand side of Equation 3 represents the initial state during an assumed time step for the aerosol generation calculation. Raoult's law (Equation 4) expresses the FP vapor mole fraction ($\tilde{y}_{v,i}$) in terms of the aerosol mole fraction ($\tilde{y}_{a,i}$). The bisectional method [11] was used to solve the total FP vapor mole fraction (x) at the current time step, $t_o+\Delta t$, in Equation 7. The mole fractions of group-i FP vapor and aerosol (Equation 8) can be obtained using the calculated $\tilde{y}_{v,i}$, $\tilde{y}_{a,i}$, and x. The aerosol generation was finally calculated by Equation 9, where Δt was the time step used in the numerical integration. The explicit scheme was used to solve the first-order differential equation (Eq. 1) in the COMPASS-FP module.

$$\tilde{x}\tilde{y}_{v,i} + \left(1-\tilde{x}\right)\tilde{y}_{a,i} = \tilde{x}_o\tilde{y}_{v,io} + \left(1-\tilde{x}_o\right)\tilde{y}_{a,io} \quad (3)$$

$$\tilde{y}_{v,i} = \tilde{y}_{a,i}\frac{P_{sat,i}(T)}{P_v} = \tilde{y}_{a,i}\eta_i \quad (4)$$

$$\tilde{y}_{a,i} = \frac{\tilde{x}_o\tilde{y}_{v,io} + \left(1-\tilde{x}_o\right)\tilde{y}_{a,io}}{\tilde{x}\eta_i + \left(1-\tilde{x}\right)} \quad (5)$$

$$\sum_i \tilde{y}_{a,i} = 1 \quad (6)$$

$$\sum_i \frac{\tilde{x}_o\tilde{y}_{v,io} + \left(1-\tilde{x}_o\right)\tilde{y}_{a,io}}{\tilde{x}\eta_i + \left(1-\tilde{x}\right)} = 1 \quad (7)$$

$$\tilde{m}_{v,i} = \tilde{y}_{v,i}\tilde{m}_v = \tilde{y}_{v,i}\tilde{m}_{total}\tilde{x} \quad (8)$$

$$G_i = \frac{\tilde{m}_{v,i_0} - \tilde{m}_{v,i}}{\Delta t} \quad (9)$$

Figure 3 shows the predicted aerosol mass by the aerosol generation model based on the homogeneous nucleation assumption and Raoult's law when the FP vapors from the reactor core at 2073 K and 8.0 MPa are discharged into the RCS where its assumed temperature and pressure are 2035 K and 7.48 MPa, respectively. This calculation was performed only to confirm that the dependency of the aerosol generation of the 8 FP groups on their thermodynamic properties (Table 2) are correctly captured.

3. Aerosol transport model

The aerosol starts to flow with the steam and hydrogen

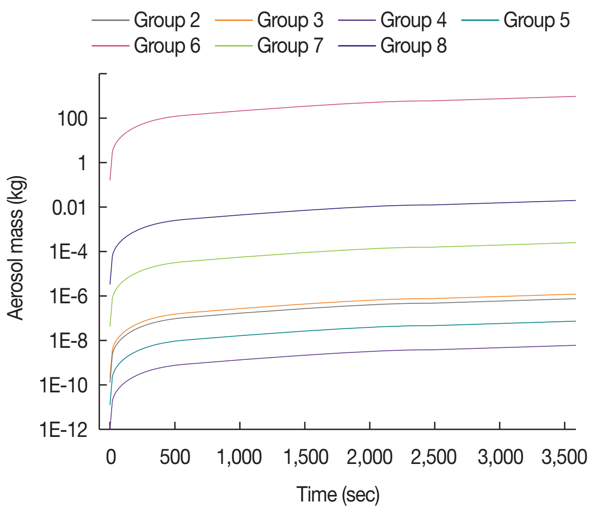

Fig. 3. Predicted aerosol mass by the COMPASS-FP module.

streams along the RCS loop during or after the aerosol generation process. However, the aerosol in the mixture flow may be deposited on the RCS wall by various mechanisms such as gravitational settling (λ_{sed}), inertia deposition (λ_{imp}), diffusiophoresis (λ_{diff}), and thermophoresis (λ_{th}). The total removal rate (λ_t) in Eq. 1 is the summation of four mechanisms as Equation 10.

$$\lambda_t = \lambda_{sed} + \lambda_{imp} + \lambda_{diff} + \lambda_{th} \tag{10}$$

The gravitational settling, sedimentation, simulates the aerosol falling down to the bottom floor due to gravity according to its mass increase through a coalescence process in the relatively high aerosol concentration region. We use the dimensionless aerosol removal rate constant for the gravitational settling as a function of the dimensionless suspended mass concentration on the basis of the test data and numerical analysis results [12]. In Figure 4, the upper solid curve (Equation 11) and the lower dashed curve (Equation 12) represent the dimensionless removal rate constant for the sedimentation under steady state conditions and decay conditions. The steady state condition means that the loss rate of aerosol mass by the sedimentation is balanced by the supply rate of the aerosol source. The decay means the transient condition which starts from a steady state due to sudden absence of the aerosol source. The removal rate constant for the sedimentation (λ_{sed}) can be obtained by substituting M_{sed} (Equation 13) and Λ_{sed} (Eq. 13) into Eq. 11 and 12.

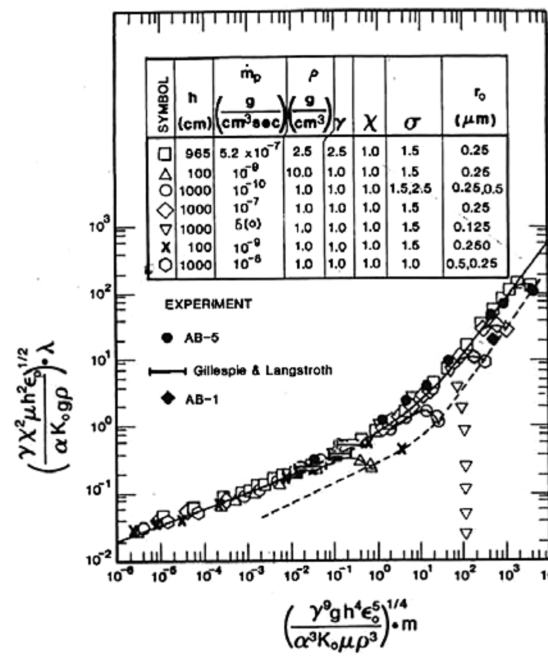

Fig. 4. Dimensionless aerosol removal rate constant for sedimentation as a function of dimensionless suspended mass concentration [12].

$$\Lambda_{sed}^{D} = 0.528 M_{sed}^{0.235} \left(1 + 0.473 M_{sed}^{0.754}\right)^{0.786} \tag{11}$$

$$\Lambda_{sed}^{SS} = 0.266 M_{sed}^{0.282} \left(1 + 0.189 M_{sed}^{0.8}\right)^{0.695} \tag{12}$$

$$M_{sed} = \left(\frac{\gamma^9 g h_{eff}^4 \varepsilon_o^5}{\alpha^3 K_o \mu \rho^3}\right)^{1/4} \cdot m_p \tag{13}$$

$$\Lambda_{sed} = \left(\frac{\gamma \varepsilon_o \chi^2 \mu h_{eff}^2}{\alpha K_o g \rho}\right)^{1/2} \cdot \lambda_{sed} \tag{14}$$

Aerosol particles in the steam and hydrogen stream in the RCS loop can be removed when the aerosol collide with the bent wall due to their inertia. For modelling the inertia removal phenomenon, we also use the dimensionless aerosol removal rate constant as a function of dimensionless suspended mass concentration following Epstein and Ellison [12]. The upper solid curve (Equation 15) and the lower dashed curve (Equation 16) in Figure 5 represent the dimensionless removal rate constant for the inertia impaction under steady state conditions and decay conditions. The removal rate constant for the inertia impaction (λ_{imp}) can be obtained by substituting M_{IMP} (Equation 17) and Λ_{IMP} (Equation 18) into Eq. 15 and 16.

http://dx.doi.org/10.14407/jrpr.2016.41.3.237

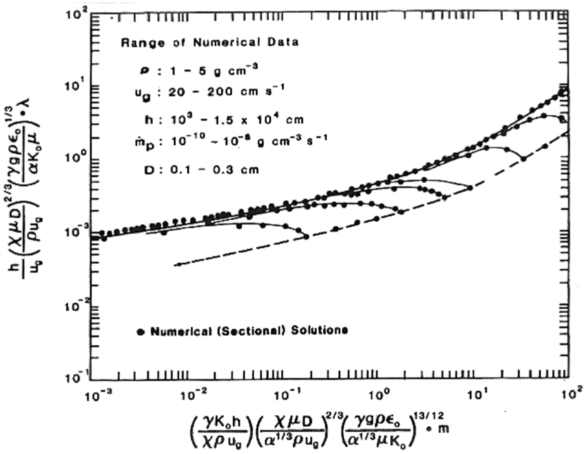

Fig. 5. Dimensionless aerosol removal rate constant for deposition by inertia impaction as a function of dimensionless suspended mass concentration [12].

$$\Lambda_{IMP}^{SS}=0.126M_{IMP}^{0.26}\left(1+2.92M_{IMP}^{1.28}\right)^{0137} \tag{15}$$

$$\Lambda_{IMP}^{D}=0.337M_{IMP}^{0.21}\left(1+1.74M_{IMP}^{0.19}\right)^{0.14} \tag{16}$$

$$M_{IMP}=\left(\frac{\gamma K_o h_{eff}}{\chi K_o u_g}\right)\left(\frac{\chi\mu D}{\alpha^{1/3}\rho u_g}\right)^{2/3}\left(\frac{\gamma g\rho\varepsilon_o}{\alpha^{1/3}\mu K_o}\right)^{13/12}\cdot m_p \tag{17}$$

$$\Lambda_{IMP}=\frac{h_{eff}}{u_g}\left(\frac{\chi\mu D}{\rho u_g}\right)^{2/3}\left(\frac{\gamma g\rho\varepsilon_o}{\alpha\mu K_o}\right)^{1/3}\cdot\lambda_{imp} \tag{18}$$

The diffusiophoresis simulates the aerosol diffusion due to the aerosol concentration gradients in a nonuniform gas mixture. This concentration gradient usually occurs around the wall surface because the aerosol vapor condenses at the colder wall. The velocity (u_{diff}) due to the diffusiophoresis may be expressed as Equation 19 where β_{12} is a mass transfer parameter using Chilton-Colburn analogy [13] and F is a FP vapor fraction of a mixture of vapor and noncondensible gas. This velocity is induced by the fission product vapor concentration gradient formed by the vapor volume reduction near the cold wall caused by the wall condensation. The removal rate constant for the diffusiophoresis (Equation 21) can be obtained by dividing diffusiophoresis velocity (u_{diff}) by the effective height (h_{eff}).

$$u_{diff}=\frac{F\beta_{12}}{\tilde{\rho}_1}\ln\left[\frac{P_v-P_1(0)}{P_v-P_1(\delta)}\right] \tag{19}$$

$$\beta_{12}=\frac{D_{12}\tilde{\rho}_1}{\delta} \tag{20}$$

$$\lambda_{diff}=\frac{u_{diff}}{h_{eff}} \tag{21}$$

The thermophoresis accounts for the movement of the aerosol particles suspended in the gas flow toward a cooler temperature region resulted from local differences in the internal energy of the gas. We use the velocity due to the thermophoresis (Equation 22) proposed by Epstein [14]. The removal rate constant for the thermophoresis can be obtained by dividing the thermophoresis velocity (u_{th}) by the effective height (h_{eff}). The effective height is defined as the ratio of volume to surface area of the control volume.

$$u_{th}=\frac{\mu\kappa}{\chi\rho_g L}\left[\frac{T_\infty}{T_w}-1\right]\left[\frac{1-(\kappa\,\mathrm{Pr})^{1.25}\left(T_w/T_\infty\right)}{1-(\kappa\,\mathrm{Pr})^{1.25}}\right]\mathrm{Nu} \tag{22}$$

$$\lambda_{th}=\frac{u_{th}}{h_{eff}} \tag{23}$$

Results and Discussion

The gravitational settling model in the COMPASS-FP module was first validated against the Aerosol Behavior Code Validation and Evaluation (ABCOVE-5) test data performed at the Hanford Engineering Development Laboratory [15] because the gravitational settling is the most dominant phenomenon in the aerosol behavior.

1. ABCOVE-5 test condition and results [14]

The ABCOVE-5 test was conducted by injecting a strong aerosol source generated by a sodium spray fire in the Containment System Test Facility (CSTF) vessel simulating a Liquid Metal Fast Breed Reactor (LMFBR) (Figure 6). The CSTF vessel was made by carbon steel and its dimensions are a diameter of 7.62 m, height of 20.3 m, and volume of 852 m^3. The sprayed 223 kg of sodium over a period of 872 s through two spray nozzles was converted into a 60% Na_2O_2 and 40% NaOH aerosol. The test conditions are summarized in Table 3. The measured maximum suspended mass concentration of the aerosol was 170 $g\cdot m^{-3}$, which was attained 383 s after the initiation of the sodium spray (Figure 7). The suspended aerosol concentration then decreased to a steady state value of 110 ± 17 $g\cdot m^{-3}$ during the spray injection. After stopping the sodium spray injection, the aerosol mass was continually decreased to 0.001 $g\cdot m^{-3}$ at about 200,000 s.

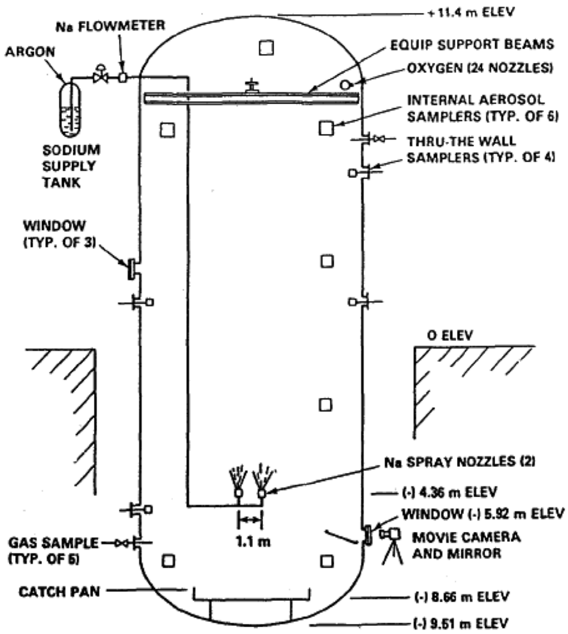

Fig. 6. Containment system fest facility [15].

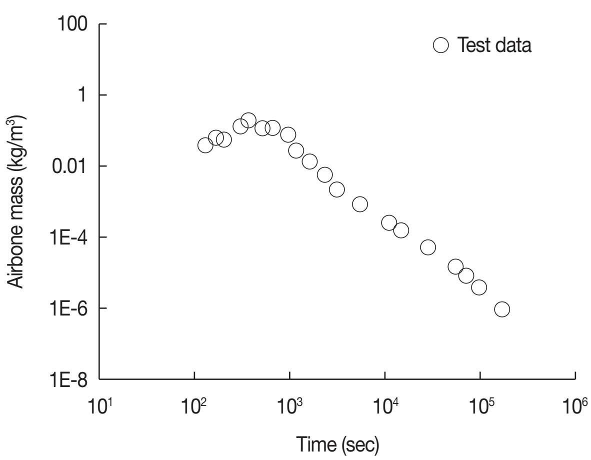

Fig. 7. Aerosol mass concentration in the atmosphere of the test facility [15].

It is believed that the thermal-hydraulic conditions including temperature and pressure in the ABCOVE-5 test represent the RCS condition for a Loss of Coolant Accident (LOCA) sequence under the severe accident. According to the thermal-hydraulic calculation results by Compass-Safety and Performance Analysis CodE for nuclear power plants (CSPACE) for simulating the severe accident of Advanced Power Plant 1,400 MWe (APR1400), the range of temperature and pressure in the RCS are 400 K–1,500 K and 100 kPa–200 kPa, respectively [16].

Table 3. Test Condition of ABCOVE-5 [15]

Initial Condition	
- Temperature	302.25 K
- Pressure	0.122 MPa
- Dew point	289.15 ± 2 K
Na Spray	
- Na spray rate	256 ± 15 $g \cdot s^{-1}$
- Spray start time	13 s
- Spray stop time	885 s
- Total Na sprayed mass	223 ± 11 kg
- Na Temperature	836.15 K
O_2 Concentration	
- Initial O_2 concentration	223 ± 11 kg
- Final O_2	223 ± 11 kg
- O_2 injection start	60 s
- O_2 injection stop	840 s
- Total O_2 mass	47.6 m^3 (STD)
Containment Condition	
- Max. avg. atmosphere temperature	552.15 K
- Max. avg. steel vessel temperature	366.65 K
- Max. pressure	213.93 kPa
- Final dew point	271.65 K
Aerosol Generation	
- Generation rate	445 $g \cdot s^{-1}$
- Mass ratio, total to Na	1.74
- Material density	2.50 $g \cdot cm^{-3}$
- Source mass median radius	0.25×10^{-6} m

2. COMPASS-FP calculation results

The COMPASS-FP module was simplified to simulate the ABCOVE-5 test results because the gravitational settling was the dominant process over the aerosol removal mechanisms. Only the single aerosol component, a mixture of Na_2O_2 and NaOH, was used in ABCOVE-5, which may not be generated in the PWR severe accident. Thus, we did not simulate the aerosol generation process but simply used the aerosol generation data given in Table 3. A single control volume simulating the ABCOVE-5 test facility was used for the COMPASS-FP calculation. The aerosol inflow ($W_{Ai, in}$) and outflow ($W_{Ai, out}$) terms in Eq. 1 were neglected because the test was performed in a confined single volume. Therefore, the governing equation for predicting the aerosol mass change can be simplified to Equation 24.

$$\frac{dm_A}{dt} = G - \lambda_{sed} m_A \qquad (24)$$

To solve Eq. 24, the steady state and decay removal rate constants for the sedimentation (Equations 11 and 12) were separately applied to λ_{sed} considering the aerosol injection period (13 s to 885 s) in the transient calculation from 13 s to

 http://dx.doi.org/10.14407/jrpr.2016.41.3.237

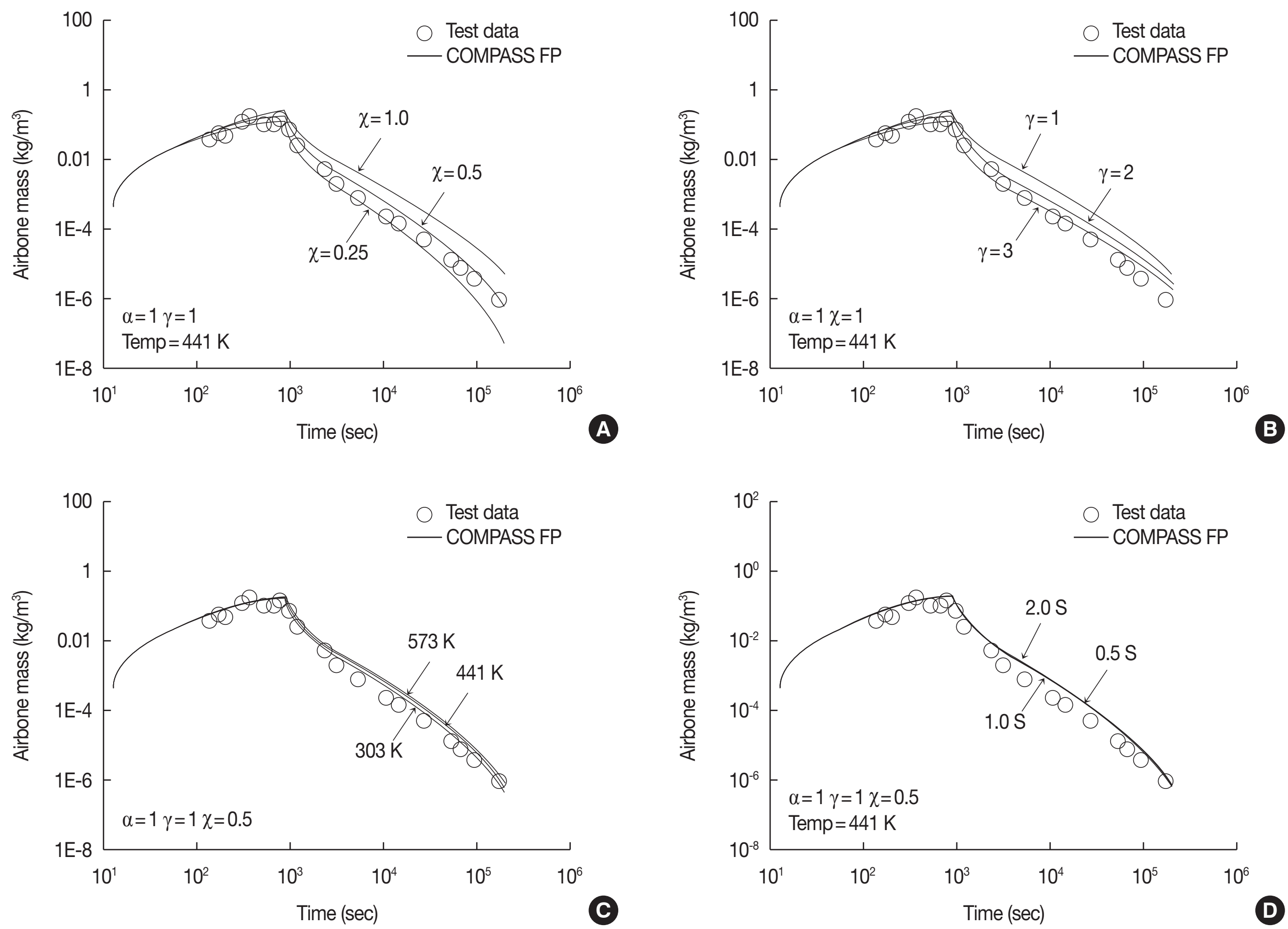

Fig. 8. (A) Calculation results for various dynamic shape factors (χ), (B) calculation results for various collision shape factors (γ), (C) calculation results for various atmosphere temperatures, and (D) calculation results for various time step sizes by COMPASS-FP module.

200,000 s. The geometric data of the test facility, volume and height, were used to calculate the effective height (h_{eff}) and the density of the aerosol cloud (m_p) in Equations 13 and 14. However, the COMPASS-FP module cannot simulate the atmosphere temperature variation because the FP module is not yet connected with the thermal hydraulic module of the COMPASS. Thus, the average temperature of 441 K in the measured data was used for calculating the temperature dependent properties in the COMPASS-FP module analysis.

The calculation result by the COMPASS-FP module by assuming the spherical aerosol shape ($\chi=1$, $\gamma=1$) [17] was overestimated about 7 times when compared to the test data (Figure 8A). To reduce the prediction error range, the sensitivity calculations by changing the dynamic shape factor from $\chi=1$ to $\chi=0.5$ and 0.25 were performed. The prediction results by the FP module with $\chi=0.5$matches the test data with the error range to approximately ±6% (Figure 8A). This may be explained by the fact that the aerosol shape is not maintained as the sphere when the aerosol falls down owing to the sedimentation duration of the test period. To see the effect of the collision shape factor (γ) on the suspended aerosol mass, the sensitivity calculation was performed by varying the collision shape factor among 1, 2, and 3. The sensitivity calculation results (Figure 8A) show that the predicted results with $\gamma=2$ or $\gamma=3$ are closer to the test results than that with $\gamma=1$. This also may mean that the aerosol shape varied from a sphere to a complex shape during the experiment.

The sensitivity calculations for the three atmosphere temperatures of 303 K, 441 K, and 573 K was performed to see the effect of the temperature dependent properties on the suspended aerosol mass. The results show that the temperature difference of 270 K does not affect the predicted aerosol mass. In addition, the sensitivity calculation results with the various time step size of 0.5 s, 1.0 s, and 2.0 s for the first-order differential equation (Eq. 1) shows almost the same results for the suspended aerosol mass.

Conclusion and Further Work

We developed the COMPASS-FP module which consists of a fission product release model, an aerosol generation model, and an aerosol transport model. In the fission product release model there are three submodels based on empirical correlations, and they are used to simulate the fission product gases released from the reactor core. In the aerosol generation model, the mass conservation law and Raoult's law are applied to the mixture of vapor and droplets of the fission products in a specified control volume to find the generation of the aerosol droplet. In the aerosol transport model, empirical correlations available from the open literature are used to simulate the aerosol removal processes owing to the gravitational settling, inertia impaction, diffusiophoresis, and thermophoresis. From the COMPASS-FP module analysis results for the suspended aerosol mass concentration of the ABCOVE-5 test, we found that the gravitational settling model in the COMPASS-FP module can accurately predict the suspended aerosol mass with an error range of about ±6% if the collision shape factor and dynamic shape factor are properly chosen considering that the aerosol shape may be changed from a sphere to a complex shape during the aerosol coagulation process. In addition, we found that the FP gases release model and the aerosol generation model in the COMPASS-FP module produced reasonable results. However, more validation for the COMPASS-FP module should be performed and connected with the thermal hydraulic solver before applying the COMPASS-FP module to a real nuclear power plant.

Acknowledgements

This work was supported by the Nuclear and Development of the Korea Institute of Energy Technology Evaluation and Planning (KETEP) grant funded by the Korea government (Ministry of Trade, Industry, and Energy) (No. 2014 1510101671).

References

1. Randall Gauntt, et al. Fukushima daiichi accident study (status as of April 2012). Sandia National Lavoratories Report SAND 2012-6173.
2. Bae JH, Park JH, Kim JT, Park RJ, Rhee BW, Song JH, Kim DH. The verification/validation report for the core heat-up module. KAERI TR-5694. 2014;1-33.
3. Han TY, Hong SJ, Hwang SH, Lee BC, Byun CS. Object-oriented programming in the development of containment analysis code. The Korea Nuclear Society Spring Meeting, Jeju Korea. May 21-22, 2009.
4. Kuhlman MR, Meyer RO. CORSOR user's manual. Battelle's Columbus Laboratories Report NUREG/CR-4173. 1985;1-14.
5. Lorenz RA, Collins JL, Malinauskas AP, Kirkland OL, Towns RL. Fission product release from highly irradiated LWR fuel. Oak Ridge National Laboratory Report NUREG/CR-0772. 1980;100-106.
6. Lorenz RA, Osborne MF. A summary of IRNL fission product release tests with recommended release rates and diffusion coefficients. Oak Ridge National Laboratory Report NUREG/CR-6261. 1995;16-23.
7. Soffer L, Burson SB, Ferrell CM, Lee RY, Ridgely JN. Accident source terms for light-water nuclear power plant. U.S. Nuclear Regulatory Commission Report NUREG/1465. 1995;5-14.
8. Cho CS, et al. APRIL.MOD3 computer code-user manual. RPI report. 1990;1-22.
9. Barin I, Knacke O. Thermochemical properties of inorganic substances. 1st Ed. Berlin Germany. Springer-Verlag. 1973;552-634.
10. Collier JG, Thome JR. Convective boiling and condensation. 3rd Ed. Gloucestershire UK. Clarendon Press. 1994;536-537.
11. Press WH, Teukolsky SA, Vetterling WT, Flannery BP. Numerical recipes. 3rd Ed. Cambridge UK. Cambridge University Press, 2007;445-448.
12. Epstein M and Ellison PG. Correlations of the rate of removal of coagulating and depositing aerosols for application to nuclear reactor safety problems. Nucl. Eng. Des. 1988;107:327-344.
13. Lahey RT, Moody FJ. The thermal-hydraulics of a boiling water nuclear reactor. 2nd Ed. La Grange Park IL. American Nuclear Society. 1993;401-409.
14. Epstein M, Ellison PG. Thermophoretic deposition of particles in nature convection flow from a vertical plate. J. Heat Transfer. 1985;107:272-276.
15. Souto FJ, Haskin FE, Kmetyk LN. MELCOR 1.8.2 assessment: aerosol experiments ABCOVE AB5, AB6, AB7, and LACE LA2. Sandia National Laboratories Report SAND94-2166. 1994;4-49.
16. Lee TB, Lee DK, Lee HS, Lee GW, Choi TS, Park RJ, Kim DH. Preliminary evaluation of CSPACE for a station blackout transient in APR1400. The Korea Nuclear Society Spring Meeting, Jeju Korea, May 12-13, 2016.
17. Fuchs NA. The Mechanics of aerosol. 2nd Ed. New York NY. Dover Publication. 1989;288-338.

http://dx.doi.org/10.14407/jrpr.2016.41.3.237